Simple sub-50-ps rise-time high voltage generator

M. M. Kekez
Institute for Information Technology, National Research Council of Canada, Ottawa K1A OR6, Canada

(Received 10 April 1991; accepted for publication 4 September 1991)

This article relates to the development of an ultrafast (nanoseconds–picoseconds time scale) compact system(s) readily applicable to the field of EMP/radiation, x-ray-induced nondestructive testing, plasma fusion (energy) experiments, bioelectromagnetic (food-drug) sterilization, drivers for x-ray preionized XeCl laser and similar applications. The present work shows that the Marx and the Pulse forming section can be integrated into a single unit. The stray capacitance present in each stage acts as a peaking capacitor. For a charging voltage per stage of <40 kV, the rise time of the output pulse is below 50 ps at 200 kV into a 100-Ω load. Work is in progress to extend the voltage amplitude to 1.6 MV while maintaining the relative pulse waveform. With a contemporary optical diagnostic technique it is believed that the present concept may achieve 1–10 ps rise-time pulses at a megavolt level in "smart gas mixtures." In addition a solution for the classical peaking circuit has been obtained and presented in the Appendix.

I. INTRODUCTION

Modern energy storage systems for the applications indicated in the abstract use Marx generators to supply the energy at (up to) 30-MV voltages, in the form of fast (as small as 5–20 ns) rise-time electrical pulses.

Usually, a Marx generator forms the first section of the energy storage system (Fig. 1) in most experimental setups.

To achieve energy compression (to enhance the pulsed power by decreasing its pulse duration) as well as to shorten the rise time, the energy from the Marx generator is fed into a pulse forming networks. The latter constitutes the second section of a system, where the energy is compressed by means of an intermediate storage (peaking) capacitor and of a gas switch to be followed by additional peaking sections composed of pulse-forming lines and peaking switches. In some systems,[1–3] the pulse forming lines are connected in series by a magnetically insulated transmission line (MITL) to form a high voltage source to energize the load.

An alternative method of sharpening the rise time of the impulse is the sole use of only magnetically isolated vacuum transmission lines.[4] There, an electromagnetic wave propagating along the structure initiates electron emission (as in a vacuum diode). This emission, at some value of the voltage and current of the leading edge of the wave, may draw sufficient current in the transmission line to achieve the cutoff condition, turning emitted electrons behind the leading edge of the wave back towards the cathode. Under these circumstances, the power pulse propagates down the transmission line and the slowly rising voltage wave front is removed by erosion by the initial emitted electrons.

In addition, some work was done to explore the feasibility of using very thin metallic foils as opening switches operating in the 1–10 ns time regime.[5] The object is to pulse sharpen and perhaps step-up the output of the pulsed power source in order to generate a very fast, Gaussian voltage pulse for single shot applications. The foils (fuses) serve to shunt current in the vacuum insulated transmission line until the fuses burst, and produce an open circuit voltage pulse given by the product of the current times the characteristics impedance of the line.

When the Marx system is coupled to a magnetically insulated vacuum transmission line to sharpen the rise time of the Marx system by a factor of 2–5 times and a vacuum diode generating a high (>100 kA) electron beam is added to provide the input to the metallic foil's structure, an output pulse as narrow as 1.1-ns full width at half maximum (FWHM) can be obtained. The usefulness of such a system appears to be limited by the need to support the thin foils with an insulating substrate.

The following U.S. patents describe systems of enhancing the rise time of pulse generator systems: U.S. patent No. 4 494 011 by Davis, U.S. patent No. 4 546 268 by Caldwell *et al.*, and U.S. patent No. 4 549 091 by Fahlen *et al.*

The Davis' system uses a high voltage avalanche source, a plurality of biased triode amplifier tubes and circuits and a voltage step-down transformer between any two consecutive tube stages to form a new pulse generator. The Davis' system has a high voltage pulse generator which provides pulse voltages in the kV range with rise times of 200 ps.

The system of Caldwell *et al.* consists of a transistor circuit and is capable of generating subnanosecond pulses. The system of Fahlen *et al.* consists of an excitation circuit for gas lasers which includes a cascade of magnetic charging circuits formed with saturable inductor switches.

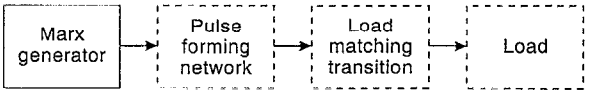

FIG. 1. Basic structure of pulsed power energy storage system.

 0034-6748/91/122923-08$02.00

II. FORMULATION

The purpose of this article is to offer a more economical approach to the development of energy storage systems with enhanced rise time characteristics on subnanosecond–picosecond time scale for multishot ($>10^7$) applications.

The Marx generator can be viewed as a distributed transmission-storage line, consisting of n-cascaded stages as shown in Fig. 2. Each stage is comprised of an energy storage capacitance C, a series inductance L (that includes the inductance of connecting the leads, the internal inductance of the storage capacitor as well as the inductance of the closing switch channel, L_1) a time-delayed switch closing at predetermined time t_0 and the peaking capacitance C_s which in our configuration is formed between the electrode of the switch and the outer enclosure of the system. Stage n is terminated by a resistive load R. The capacitors C are charged in parallel through the charging resistors (shown in Fig. 2) to a voltage V.

To clarify the overall task, we consider a single stage of the Marx generator with the load R, representing the classical formulation of the peaking circuit (Fig. 3).

A. Analysis of peaking circuit

The solution of the circuit equations is quite involved and is included as Appendix A. This sections will summarize the initial equations and important results.

Referring to Fig. 3, we start with both switches open and the capacitor C charged to a voltage V. When switch No. 1 is closed, the components L, C, and C_s are placed in series. At any time after closing the first switch, the charge at C is

$$q(t)=Q\left(1-\frac{C_s}{C+C_s}(1-\cos\omega t)\right) \tag{1}$$

where

$$Q=VC$$

and

$$\omega^2=\left(\frac{1}{C}+\frac{1}{C_s}\right)\Big/L.$$

From Eq. (1), we see that for $\omega t=\pi/2$ and $C_s \ll C$ then the charge at C_s equals VC_s, i.e., voltage V at C has been

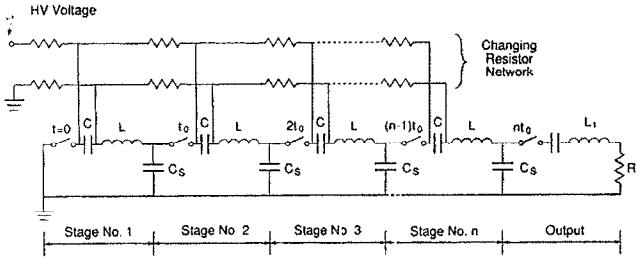

FIG. 2. Schematic of Marx.

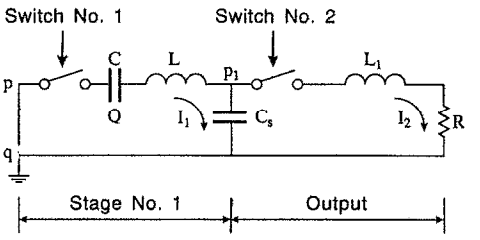

FIG. 3. Peaking system circuit.

transferred to C_s. Also for $C_s \ll C$ *the voltage across* C *remains essentially constant and can be represented by a dc source.*

Suppose that switch No. 2 is now closed at $t=t_0=\pi/(2\omega)$, and assume that load R is the input impedance of the second stage of the Marx generator and/or that of the load.

From Appendix A, the current i_2 is given by the sum of nonoscillating and oscillating solutions (A10 and A12).

The nonoscillating portion depicts a wave form that starts with a finite slope at $t\geqslant 0$ and has a rise time (10%–90%) of

$$\tau_r=2.2L_1/(\bar{k}R), \tag{2}$$

where L_1 is the inductance of the switch and $\bar{k}$ is a slowly varying function of L, L_1, R, and C_s as shown in Fig. 4.

If only the leading edge and flat top portion of the waveform are of interest, the nonoscillating portion of i_2 can be approximated as

$$i_2(\text{non-osc})=(V/R)[1-\exp(-\bar{k}Rt/L_1)]. \tag{3}$$

The relative amplitude of the oscillating portion of i_2 will now be evaluated from Eq. (A12). There, the second

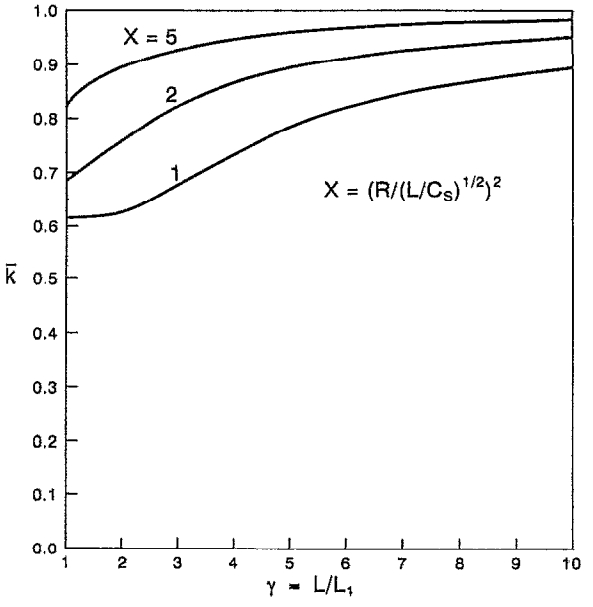

FIG. 4. $\bar{k}$ vs γ.

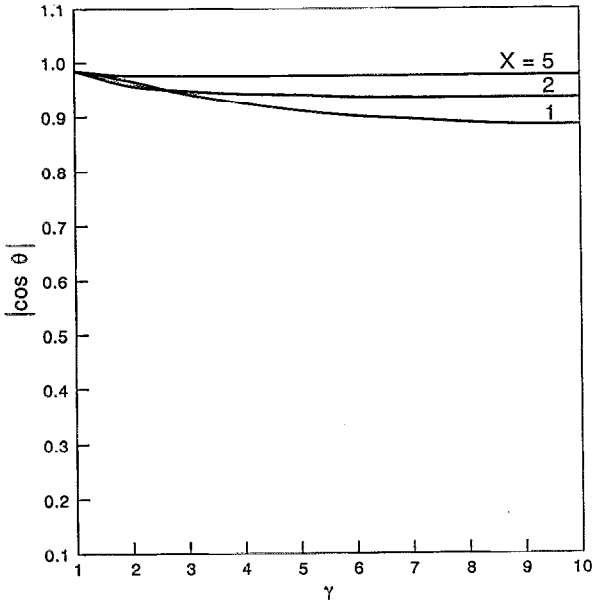

FIG. 5. $|\cos\theta|$ vs γ.

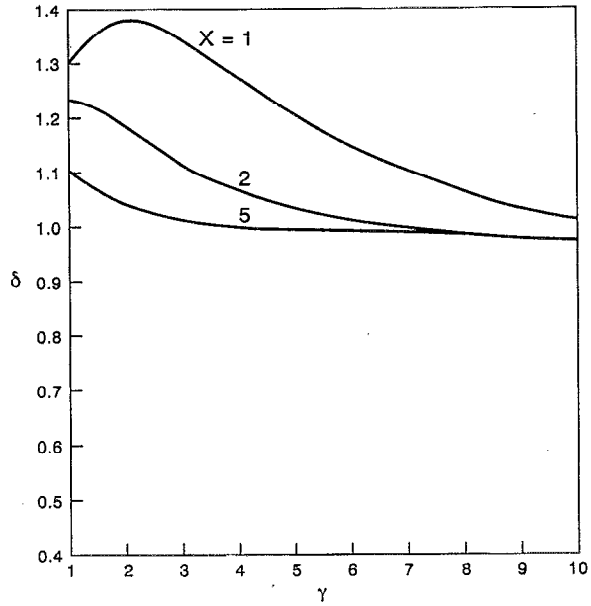

FIG. 7. δ vs γ.

oscillating term dominates. For $\Omega t+\theta=\pi/2$ (and/or $=5\pi/2$), $\sin(\Omega t+\theta)=1$ and as $\exp(m_0 t)\simeq 1$, the relative amplitude of this oscillation, "a" is

$$L_1\Omega/\bar{k}R|\cos\theta|\cong a,$$

and the rise time (10%–90%),

$$\tau_r\cong 2.2(L_1/\bar{k}R)=1.1(a|\cos\theta|/\pi)T, \qquad (4)$$

where both T (the oscillation period) and a are deduced from measurements. The theoretical value of $|\cos\theta|$, the amplitude a, X and δ are given in Figs. 5, 6, and 7 in terms of γ and X.

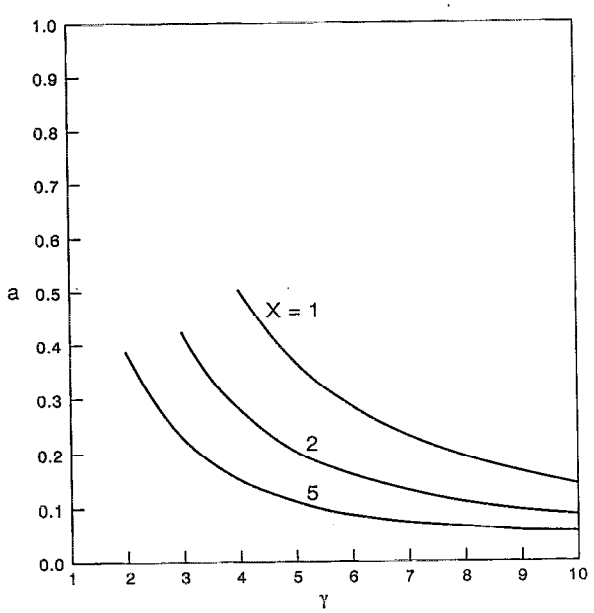

FIG. 6. Amplitude a vs γ.

B. Analysis of the Marx distributed network

Equation (3) suggests that the peaking arrangement of the voltage across C_s (between points p_1 and q) is equivalent to that of a very small internal impedance voltage source energizing the series combination of L_1 and R when $\bar{k}\cong 1$. Since

$$t_0=(\pi/2)(LC_s)^{1/2}\gg L_1/R,$$

the leading edge and the top portion of the pulse for the Marx distributed network can now be related to that of the peaking circuit arrangement. For example, for a two-stage Marx it is necessary to replace R terminating the first stage, with the impedance of the Marx arrangement $=(L/C_s)^{1/2}$ [making X of Eq. (A6a) equal 1], and to replace the output after the second stage. Alternatively one may remove the lead pq and insert the voltage source: $V[1-\exp(m_1 t)]$ in its place. Hence stage No. 1 becomes the second stage.

By expanding this procedure to n stages, and assuring that subsequent switches in the system will close at a time which is a multiple of t_0, our formulation yields the output voltage to be

$$V_{\text{out}}=nV(e^{-nt/CR}-e^{-\bar{k}Rt/L_1}).$$

To examine this idea in further detail, a computer simulation was carried out using the microcomputer analysis program.[6] The results are given in Fig. 8. There is no significant difference in the waveform between a single stage and, say the seventh stage and/or any other number in between.

However, the computer runs were not sufficiently precise to permit the determination of the decrement coefficient of the damped oscillation governed by Eq. (A8). A new computer program which has shown great promise[7] will be employed in the future.

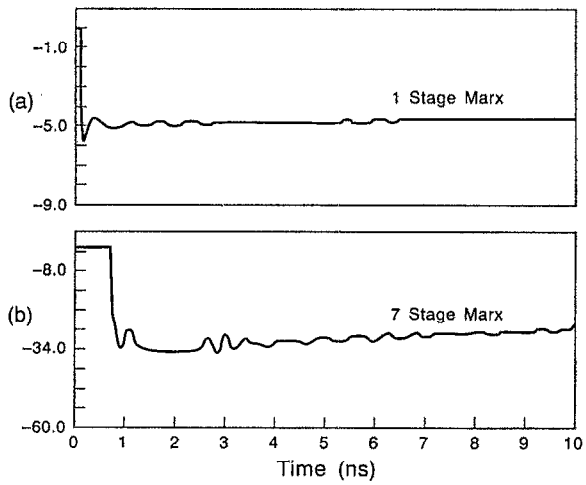

FIG. 8. Computer simulation for (a) the peaking capacitor circuit and (b) 7 stage Marx with $R = 100\ \Omega$, $L = 4$ nH, $\gamma = 4$, $C = 2.7$ nF, $C_s = 1.1$ pF, and $V = 5$ units and $t_0 = 0.104$ ns.

III. DESIGN

In the light of the discussed formulation, the following five criteria are incorporated in the design.

(1) The generators are designed in the form of a coaxial structure. Thus the energy storage capacitors, connecting leads, and metallic enclosures (acting as a return conductor), lead to the establishment of a fast pulse forming line. This arrangement offers:

(a) simplicity of construction and small (compact) size,

(b) ease of scaling up to a larger pulsed power system,

(c) low inductance of single stage, and

(d) minimum of potential electromagnetic pulse health hazards to workers in the laboratory proximal to large high voltage generators. For lethal effect of high electric pulses (2–20 kV/cm) on bacteria and yeast cell see Ref. 8, for overall review of the bio-electromagnetic effects of electromagnetic pulse[9] and other applications.[10]

(2) As the analysis presupposes a constant value of the peaking capacitors with increasing voltage rate (up to the Marx voltage output level), it was decided to let C_s to be determined by the coupling between the electrodes of the switch and the Marx metallic enclosure. If this electrode is a sphere of radius r_0 and the enclosure (plane) is at infinity, then $C_s = 4\pi\epsilon_0 r_0$. A potential (electrostatic) theory was used to compute the value of C_s in the chosen geometry.

(3) Optically controlled sequencing of the Marx is employed. This is achieved by arranging each stage to provide a hard UV source to photoionize each consequent stage of the bank. The object is to ensure:

(a) Rapid and spatially uniform avalanche development for the abnormal glow-type discharge is employed and is capable of carrying large (< 100 Å) current before the onset of the spark channel.[11] As the pressure of the gas in the (spark gap) switch increases, the abnormal glow phase becomes very short in duration. Even if the applied voltage across the gap is much higher than the static breakdown voltage, this (glow) phase will be present as long as UV preionization is of sufficient magnitude.

Mixtures of two or more gases (with additives) offers an opportunity to manipulate the chemical kinetics and tailor the gas mixture to achieve best switching performance. Some of these "smart gas composition" have been designed for high conductivity in the "on" state and fast recovery.[12,13]

(b) Although the effective ionization range of the radiation from single spark (arc) source as indicated by its ability to induce or initiate a secondary isolated discharge can be several tens of centimeters at atmospheric pressure,[14] more recent UV photoionization measurements using an x-band microwave interferometer[15] show that such a (photoionized) plasma density is a function of both the gas mixture and the irradiation source parameters, in some "smart gas" mixtures.

As far as our design goals are concerned, it is required ideally that the time differences between the onset of the spark channels in two adjacent spark gaps be equal to t_0.

(4) To ensure ease of portability as well as stationary application, the decision was made that each of the Marx stages be charged up to 40 kV. This assures that the weight of the system be minimized by avoiding an oil-filled enclosure for the dc power supplies. For this voltage range there is a wealth of scientific data concerning the breakdown characteristics evaluated from the macroscopic and atomic point of view.

For example, four decades ago Fletcher[16] constructed an impulse generator system capable of delivering 20–50 kV impulses with a rise time of 0.4 ns into a high (83.3 Ω) impedance load.

Subsequently, a number of papers followed reporting similar studies. Specifically, the effect of intensity and duration of UV irradiation on the formative time lag was investigated in great detail by the Russian school (i.e., Academician G. A. Mesyats *et al.*[17]) in the late 60's.

(5) The final design aim is to strictly adhere to high-voltage (HV) engineering practice, whereby each energy storage stage is guarded by a corona ring and the joining leads are imbedded in an elastomer to protect them from debris. This permits a reliable operation of the spark gap subjected to say 80% of the self-breakdown voltage without exposing the system to the risk of prefire during operation.

IV. EXPERIMENTAL ARRANGEMENTS

The parameters of a 200-kV Petit–Marx, an earlier 1-ns rise time, 600-kV, 60-J,[18] and a 1.6-MV Marx, currently under construction, are collected and listed in Table I for comparison. The structure of the 200-kV Petit–Marx is essentially the same as those of the 1.6-MV one, and both have some resemblance to that of Platts.[19] Ceramic (barium–titanium) capacitors of 2.7 nF, 40 kV were used in our design. A conceptually similar design is adopted in an electron beam fusion experiments,[20] in an intense 3-ns neutron source[21] and for flash x-ray radiography.[22]

In Fig. 9, a cross-sectional view of the 200 kV and/or 1.6-MV Marx is shown. The spark gaps consist of 1/2-in.-

TABLE I. Characteristics of the coaxial Marx generators.

	200–320 kV	600–960 kV	1000–1600 kV
Charging voltage	25–40 kV	25–40 kV	25–40 kV
Number of stages	8	24	40
Number of capacitors	8	72	40
Capacitance per stage	2.7 nF	8.1 nF	2.7 nF
Erected capacity	0.3375 nF	0.3375 nF	67.5 pF
Load	100 Ω	100 Ω	100–350 Ω
Duration of pulse (for decay to	theory: 23.4 ns	23.4 ns	4.69–16.4 ns
50% of peak)	exp: 29.4 ns	38 ns	···
Stored energy	6.75–17.2 J	60.75–155.5 J	33.75–86.0 J

diam brass spheres placed 0.10 in. apart, and the separation between the adjacent spark gaps is about 6 cm. The insulating rail holds the capacitors and the spark gaps. The rail is supported by the 4.25-in. o.d. plexiglass. The 2.7-nF, 40-kV ceramic TDK capacitors are charged through 2-MΩ, 2-W carbon resistors. A return load in the Marx is provided by a metallic enclosure, of about 4.5-in. diameter.

To achieve reliable operation of the 1.6-MV system and to minimize the risk of breakdown between the last stage of Marx and the metallic enclosure, an additional plexiglass shell that could be pressurized differentially will be used. As pointed out in Ref. 23, where the minimum sparkover voltages were calculated from the single equation over seven decades of thin (2.5 μm) film mylar up to 35 m in air, the best kind of dielectrics are not homogeneous materials, but rather properly chosen strata of dielectrics (sandwich of dielectrics) that may exhibit synergism, i.e., a compounded sandwich may show a dielectric strength in excess of that expected from the sum of properties of separate dielectrics.

To calibrate the system, a 100-Ω, 12-in. o.d. coaxial line was used. A 13-in.-long conical coaxial transition section was built to couple the generator and the 100-Ω line. In this way the system is ideally suited for performance evaluation of

(a) annular resistive thin-film current monitors,
(b) capacitive and resistive voltage probes,
(c) shielded Faraday cup probes,
(d) pressure (piezoelectric) probes, and
(e) Rogowski coils and B-dot probes.

V. EXPERIMENTAL FINDINGS AND DISCUSSION

The generator impulse waveform was measured with a capacitive probe of a bandwidth up to 3 GHz as used in Ref. 18. This probe was installed in a 12-in. o.d. coaxial line 100-cm downstream from the generator.

For this upper bandwidth value of 3 GHz, the calculated rise time of the probe is $\tau_r = 1.1/(\pi f) = 1.1/(3\times10^9\pi) = 116$ ps. Also, τ_r can be interpreted as the time needed for a steep traveling field front to traverse the diameter of the probe of 3.2 cm: $t = 3.2$ cm$/3\times10^8$ cm/s $= 106$ ps.

The experimental data [Fig. 10(a)] show that τ_r of the system is 117 ps. Hence the rise time of the generator itself is estimated to be $(117^2 - 106^2)^{1/2} = 49.5$ ps (worst scenario). Using the same formula and applying it to the rise time of the probe, we get the rise time of the generator to be $(117^2 - 116^2)^{1/2} = 15.3$ ps. Any minor error in τ_r measured, implies that this result should be treated with some caution. An alternative approach is to use Eq. (4).

From Fig. 10(a) we measure a maximum relative amplitude of oscillation, $a = 27.5\%$ and that $T = 0.275$ ns. From Fig. 5, we see that the plots of $|\cos\theta|$ vs γ with X as a parameter are flat curves. In zero order approximation $\cos\theta = 1$. However, for our design: $X = 2.75$ and $\gamma = 4$ we get $\cos\theta = 0.965$ from which with Eq. (4), the result is: $\tau_r = 25.6$ ps.

Such values of τ_r are not surprising. In Ref. 24, the self inductance of the switch in a carefully designed 50-Ω system was measured to be in the range of 0.6–0.8 nH, where the gap was pressurized to 2–5 atmosphere of N_2 which provided 4-kV breakdown levels.

Taking this value for L_1, the first part of Eq. (4) can be used to supply another estimate of the rise time. For $X = 2.75$, $\gamma = 4$, from Fig. 4, we get the coefficient $\bar{k} = 0.9$. Hence, $\tau_r = 2.44L_1/R = 24.4$ ps for $L_1 = 1$ nH and $R = 100$ Ω.

For high (≥50 Ω) impedance systems, modern pulsed power technology is capable of producing picosecond voltage impulses in the megavolt range. The significance of this capability is summarized in Ref. 25. Adopting their proposed switching medium to be of high (10–800 atmosphere) pressure gas and supplementing the design with the idea of a differential pressurization of the inner structure (so as to be still far from the stress breaking point

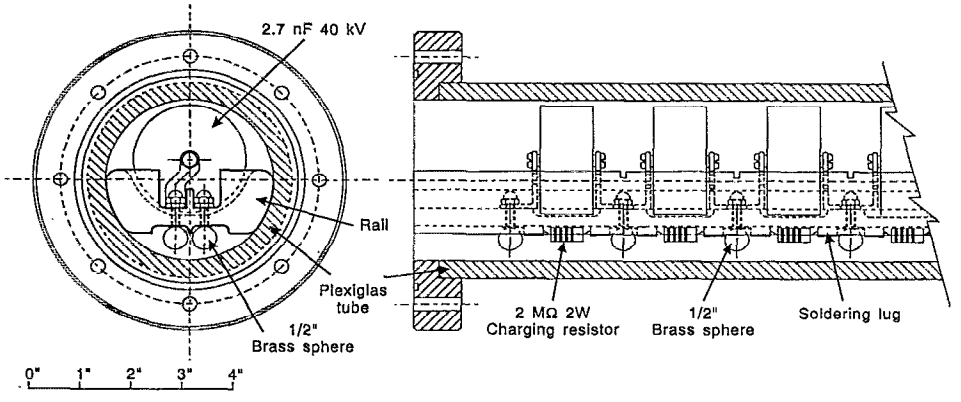

FIG. 9. Cross-section view of Marx: (a) radial and (b) longitudinal view.

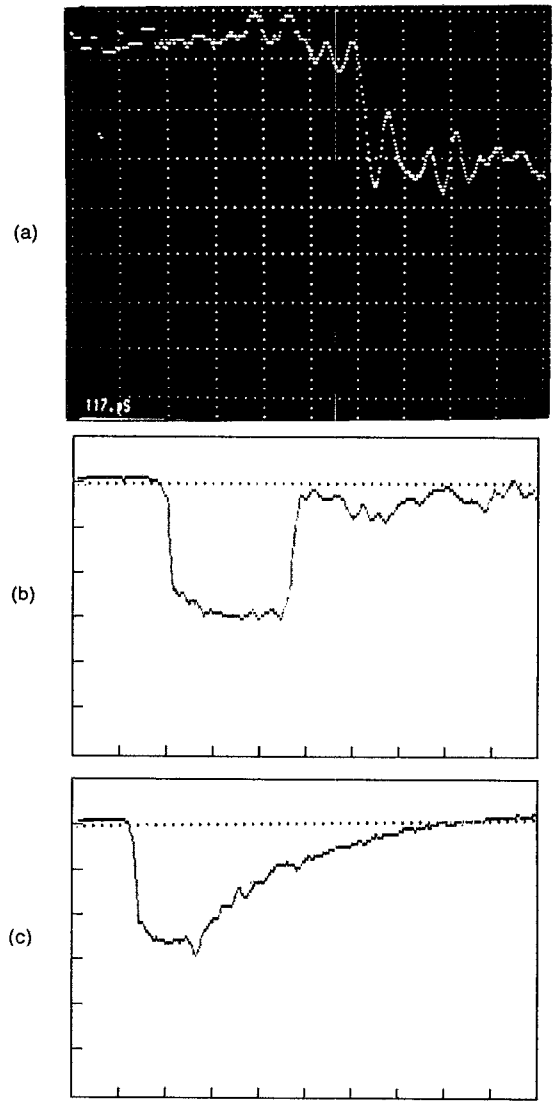

FIG. 10. 200 kV negative impulses: (a) 0.5 ns/div recorded by Textronix 6 GHz digitizer of type 7250, (b) 5 ns/div recorded by Textronix 7104 scope with 7A29 plug-in, C101 video camera, Compaq 286 computer, and Asyst Software program. (c) As in (b) but for 100 Ω "pure" resistive load. Here time scale is 10 ns/div. Capacitive-resistive load terminates a 100 Ω coaxial line. The width of the pulse is equal to double the transit time of the line (between the probe and the load).

capacity of each element), then the gap separation and the self inductance of the switch could be decreased. As in semiconductor design, the same logic applies here: to make a circuit faster, one generally must make it smaller to minimize the transit time of electrons bridging the switching medium (spark gap length), hence to minimize the lumped parameter L_1 used here to account for the many physical processes occurring in the gap.

We claim that the present work offers an additional support towards the idea of Mayhall *et al.*[25] of producing a voltage rise time between 1 and 10 ps at a sub-megavolt level, and/or even higher levels. With minor "tuning" and design variation of the present concept, a way appears to be available to achieve these goals.

One stumbling block is the diagnostics. The traditional approach which uses high speed oscilloscopes and digitizers, fails because the instrumentation has similar/or smaller bandwidth characteristics than the high voltage system under test. A possible solution to this problem is an alternative method with superior temporal resolution: short-pulse laser diagnostics that was pioneered by Auston and his team.[26] The upper limit of optics bandwidth outpaces the electronic bandwidth by about two orders of magnitude, and the use of picosecond/femtosecond laser pulse diagnostics should contribute to the advance in the field of high voltage power technology.

The reproducibility of the results given in Figs. 10(a)–10(c) is relatively good: less than 5% variation when averaged over 200 shots from day to day. In comparison to a 6 GHz digitizer, slower oscilloscopes operating on long ($\geqslant$5 ns/div) time scale are not able to record a true amplitude of the oscillation superimposed on the main pulse. Compare Figs. 10(b) and 10(c) with Fig. 10(a). Depending on the type of the load, the Marx system is also capable of generating the square and/or the double exponential pulse. [See Figs. 10(b) and 10(c).]

Measurement of the formative time lag versus the number of switches in the Marx (from 1 to 9) form a remarkably straight line and permits an accurate determination of the parameter t_0. The formative time lag is marked by the onset of the spark channel and the method used is the same as in Ref. 18.

ACKNOWLEDGMENTS

The author is indebted to Dr. N. N. Abdelmalek for his contribution to this article. Thanks are due to Mr. J. G. Dunn for his work on the experimental data acquisition. Interest in this work shown by Dr. A. S. Podgorski and Dr. M. M. C. Collins, and Mr. A. S. Mayman are fully acknowledged. The author is also indebted to Dr. C. Gardner for directing some parts of this work. Special thanks are due to the reviewer for the critique and work done to enhance the quality of the paper, in particular, by supplying computer runs on a Micro-Cap II, to check the concept of precisely timed switches and how does the Marx provide the fast output pulse. We thank him also for providing Ref. 27.

APPENDIX A: SOLUTION OF THE CIRCUIT EQUATIONS

From Fig. 2, the circuit equations are

$$L\ddot{q}_1+\frac{q_1}{C}+\frac{q_1}{C_s}-\frac{q_2}{C_s}=V$$

$$-\frac{q_1}{C_s}+L_1\ddot{q}_2+R\dot{q}_2+\frac{q_2}{C_s}=0 \tag{A1}$$

Let us introduce the following parameters

$$\omega_c^2=1/LC,\quad \omega_s^2=1/LC_s,\quad \alpha=R/L,\quad \text{and}\quad \gamma=L/L_1,$$

and eliminate q_1 in (A1), we get

$$\{D^4+\alpha\gamma D^3+[(1+\gamma)\omega_s^2+\omega_c^2]D^2+\alpha\gamma(\omega_s^2+\omega_c^2)D+\gamma\omega_s^2\omega_c^2\}q_2=\gamma\omega_s^2V/L, \tag{A2}$$

where $D=d/dt$. Equation (A2) is a fourth-order differential equation whose auxiliary equation is given by

$$f(m)=m^4+\alpha\gamma m^3+[(1+\gamma)\omega_s^2+\omega_c^2]m^2 + \alpha\gamma(\omega_s^2+\omega_c^2)m+\gamma\omega_s^2\omega_c^2=0. \quad \text{(A3)}$$

As $\omega_c^2 \ll \omega_s^2$ the constant term in Eq. (A3) is very small, and a first-order approximation to one of its roots is $m_1=0$. Using the Newton–Raphson iteration once, this root is

$$m_1=-\frac{f(m=0)}{f'(m=0)}=-\frac{\gamma\omega_s^2\omega_c^2}{\alpha\gamma(\omega_s^2+\omega_c^2)}\cong-\frac{\omega_c^2}{\alpha}=-\frac{1}{RC}. \quad \text{(A4)}$$

By extracting this root from Eq. (A3) and neglecting ω_c^2 w.r.t. ω_s^2, we get a third-degree equation:

$$m^3+\alpha\gamma m^2+(1+\gamma)\omega_s^2 m+\alpha\gamma\omega_s^2=0. \quad \text{(A5)}$$

From the first two terms of (A5), an approximate root is

$$m_2=-\alpha\gamma=-R/L_1.$$

Using Newton–Raphson iterations twice, we get

$$m_2=-\alpha\gamma\bar{k}=-R\bar{k}/L_1, \quad \bar{k}<1, \quad \text{(A6)}$$

where $\bar{k}$ is a function of γ and X, defined by

$$X=[R/(L/C_s)^{1/2}]^2=(\alpha/\omega_s)^2. \quad \text{(A6a)}$$

$\bar{k}$ is given in Fig. 4.

By extracting this root from Eq. (A3), we get the quadratic equation

$$m^2+\alpha\gamma(1-\bar{k})m+(1+\gamma)\omega_s^2-\alpha^2\gamma^2(1-\bar{k})\bar{k}=0, \quad \text{(A7)}$$

which has the complex roots

$$m_{3,4}=-\frac{\alpha\gamma(1-\bar{k})}{2}\pm j\omega_s[(1+\gamma)]^{1/2} \times\left(1-\frac{\gamma^2X(1-\bar{k})(1+3\bar{k})}{4(1+\gamma)}\right)^{1/2},$$

and may be written as

$$m_{3,4}=-[\alpha\gamma(1-\bar{k})/2]\pm j\omega_s\delta=m_0\pm j\Omega. \quad \text{(A8)}$$

The parameter δ of (A8) is given in Fig. 7 as a function of γ for $X=1$, 2, and 5.

The solution of Eq. (A1) is thus given by

$$q_2=C_1\exp(m_1t)+C_2\exp(m_2t)+C_3\exp(m_0t) \times\cos(\Omega t+\theta)+CV. \quad \text{(A9)}$$

C_1, C_2, C_3, and θ are determined from the initial conditions of q_1, q_2, i_1, i_2, and by a time-delayed action of switch No. 2 in respect to switch No. 1. Suppose that switch No. 1 is closed at $t=0$ and switch No. 2 at $t_0=\pi/(2\omega_s)$. From Eq. (1) in the text, at $t=t_0$, $i_1=V/\sqrt{L/C_s}$, i.e., if $C \ll C_s$ the charge transferred to C_s is VC_s and thus $q_2(t_0)=0$ and $i_2(t_0)=0$.

Evaluation of the constants C_1 and C_2 of (A9) reveal that the nonoscillating part of i_2 to a good approximation is

$$i_2=(V/R)[\exp(m_1t)-\exp(m_2t)]. \quad \text{(A10)}$$

If only the leading edge and flat top portion of the waveform are of interest, Eq. (A10) can be approximated as

$$i_2=(V/R)[1-\exp(-\bar{k}Rt/L_1)]. \quad \text{(A11)}$$

The damped oscillation part of (A2) is

$$i_2\equiv\frac{V}{R}\left(\frac{1-\bar{k}}{2\bar{k}\cos\theta}\cos(\Omega t+\theta) + \frac{L_1\Omega}{\bar{k}R\cos\theta}\sin(\Omega t+\theta)\right)e^{-R(1-\bar{k})t/2L_1}, \quad \text{(A12)}$$

where

$$\tan\theta=-\frac{\alpha\gamma(1-\bar{k})}{2\Omega}. \quad \text{(A13)}$$

Figure 5 gives $|\cos\theta|$ as a function of γ for $X=1$, 2, and 5. As can be seen $|\cos\theta|\sim1$ for large variation in X and γ. Thus $\theta\sim0$ and from Eq. (A13) $\tan\theta\sim0$. This happens when $\bar{k}\to1$ and further simplification can be done.

The dominant term in (A12) is the second one as $\bar{k}\to1$. Collecting the important terms for i_2 gives

$$i_2=(V/R)\{[1-\exp(-\bar{k}Rt/L_1)] + (L_1\Omega/\bar{k}R\cos\theta)\sin(\Omega t+\theta) \times\exp[-R(1-\bar{k})t/2L_1]\}. \quad \text{(A14)}$$

From Fig. 5 we see $|\cos\theta|\sim1$, $\theta\sim0$, and $\delta\sim1.1$ while as explained in Sec. 2.2 $\bar{k}\cong1$. This simplifies (A14) to

$$i_2=(V/R)\{[1-\exp(-Rt/L_1)] + (1.1L_1\omega_s/R)\sin(1.1\omega_st)\}, \quad \text{(A15)}$$

$$\frac{di_2}{dt}=\frac{V}{R}\left[\frac{R}{L_1}\exp\left(-\frac{Rt}{L_1}\right)+\frac{1.21L_1\omega_s^2}{R}\cos(1.1\omega_st)\right]. \quad \text{(A16)}$$

From Eq. (5) we find that the second term in Eq. (A16) adds little to the current rise time and

$$\frac{di_2}{dt}=\left(\frac{V}{L_1}\right)\exp\left(-\frac{Rt}{L_1}\right). \quad \text{(A17)}$$

The peaking circuit discussed here was also described in Harrison[27] (supplied by the reviewer). Harrison develops a set of equations that can be used to calculate the value of the peaking capacitance and the switching time for given values of circuit parameters. While Harrison does not provide a closed-form solution for the two mentioned unknowns, he provides a set of simultaneous equations that can be solved using a computer.

[1] J. P. Corley, D. L. Johnson, G. J. Weber, G. J. Denison, P. J. Pankuch, and J. J. Ramirez, *6th IEEE Pulsed Power Conference*, Arlington, VA (IEEE, New York, 1989), p. 486.

[2] I. Smith, R. Altes, P. Corcoran, R. Kuenning, H. Nishimoto, D. Pellow, and D. Wake, *7th IEEE Pulsed Power Conference*, Monterey, CA (IEEE, New York, 1989), p. 36.

[3] K. Imasaki, S. Miyamoto, N. Yugami, T. Akiba, K. Emura, H. Takabe, S. Nakai, and C. Yamanaka, *Laser Interaction and Related Plasma*

Phenomena, edited by H. Hora and G. H. Miley (Plenum, New York, 1988), Vol. 8, pp. 633–651.
[4]M. DiCapua, D. A. Goerz, and K. Freytag, *6th IEEE Pulsed Power Conference*, Arlington, VA (IEEE, New York, 1987), p. 393.
[5]N. E. Molau, J. E. Vernazza, R. A. Anderson, D. A. Goerz, and R. R. Heritsch, *7th IEEE Pulsed Power Conference*, Monterey, CA (IEEE, New York, 1989), p. 975.
[6]Spectrum Software, 1021 South Wolfe Rd., Sunnyvale, CA 94086.
[7]PSpice Circuit Analysis, Micro Sim Co., 20 Fairbank, Irvine, CA 92718; M. Dion (private communication).
[8]H. Huelsheger, J. Potel, and E. G. Niemann, Radiat. Environ. Biophys. **22**, 149 (1983).
[9]T. E. Aldrich, C. E. Easterly, P. C. Gailey, and C. B. Hamilton, Oak Ridge National Laboratory Report: ORNL/TM-10784, DE88 012118 (1988).
[10]J. E. Dunn and J. S. Pearlman, U.S. patent No. 4 695 472 (1987).
[11]M. M. Kekez, M. R. Barrault, and J. D. Craggs, J. Phys. D **3**, 1886 (1970); and M. M. Kekez and P. Savic, J. Phys. D **7**, 620 (1974).
[12]L. G. Christophorou, D. L. McCorkle, and S. R. Hunter, *5th Gas Dielectric Conference* (Pergamon, New York, 1987), p. 381.
[13]E. E. Kunhardt and M. G. White, J. Appl. Phys. **56**, 1391 (1984).
[14]G. R. Bainbridge and W. A. Prowse, Can. J. Phys. **34**, 1038 (1956).
[15]H. J. Sequin, J. Tulip, and D. C. McKen, IEEE J. Quantum Electron. **QE-3**, 311 (1974).
[16]R. C. Fletcher, Phys. Rev. **76**, 1501 (1949).
[17]G. A. Mesyats, Yu. I. Bychkov, and V. V. Kremnev, Sov. Phys. Usp. **15**, 282 (1972); also Yu. I. Bychkov, Yu. D. Korolev, and G. A. Mesyats, Sov. Phys. Usp. **21**, 944 (1978).
[18]M. M. Kekez, J. LoVerti, A. S. Podgorski, J. G. Dunn, and G. Gibson, *7th IEEE Pulsed Power Conference*, Monterey, CA (IEEE, New York, 1989), p. 123.
[19]D. Platts, *5th IEEE Pulse Power Conference*, Arlington, VA (IEEE, New York, 1985), p. 834.
[20]K. Takagi, Y. Kubota, and A. Miyahara, Jpn. J. Appl. Phys. **18**, 1135 (1979).
[21]J. Chang and R. J. Leeper, Rev. Sci. Instrum. **51**, 715 (1980).
[22]D. L. Fehl and J. Chang, Rev. Sci. Instrum. **54**, 665 (1983).
[23]M. M. Kekez and P. Savic, J. Appl. Phys. **69**, 7510 (1991).
[24]M. R. Barrault and M. M. Kekez, J. Sci. Instrum. **44**, 486 (1967).
[25]D. J. Mayhall, J. H. Yee, and F. Villa, *7th IEEE Pulsed Power Conference*, Monterey, CA (IEEE, New York, 1989), p. 514.
[26]D. Auston, Phys. Today, **41**, Feb., 40 (1990).
[27]J. L. Harrison, Circuit and Electromagnetic System Design Notes, Note 41 (1984), Maxwell Laboratories Inc., 8888 Balboa Avenue, San Diego, CA 92123.